Biosensors and Bioelectronics 137 (2019) 72–81

Contents lists available at ScienceDirect

Biosensors and Bioelectronics

journal homepage: www.elsevier.com/locate/bios

Photovoltaics, plasmonics, plastic antibodies and electrochromism combined for a novel generation of self-powered and self-signalled electrochemical biomimetic sensors

Ana P.M. Tavares[a,b,c], Liliana A.A.N.A. Truta[a,b], Felismina T.C. Moreira[a,b], G. Minas[c], M. Goreti F. Sales[a,b,*]

[a] BioMark/ISEP, School of Engineering, Polytechnic Institute of Porto, Portugal
[b] CEB, Center of Biological Engineering, Minho University, Portugal
[c] CMEMS, Center for Microelectromechanical Systems, Minho University, Portugal

ARTICLE INFO

Keywords:
Biomimetic sensor
Cancer biomarker
Dye-sensitized solar cells
Electrochromic cell
Carcinoembryonic antigen

ABSTRACT

This work describes further developments into the self-powered and self-signalled biosensing system that merges photovoltaic cells, plastic antibodies and electrochromic cells into a single target. Herein, the plasmonic effect is introduced to improve the photoanode features of the photovoltaic cell, a dye sensitized solar cell (DSSC), and better electrocatalytic features are introduced in the electrode containing the sensing element.

In brief, the DSSC had a counter-electrode of poly(3,4-ethylenedioxythiophene) on an FTO glass modified by a plastic antibody of 3,4-ethylenedioxythiophene and pyrrol. The photoanode had dye sensitized TiO_2 modified with gold nanoparticles (AuNPs) to increase the cell efficiency, aiming to improve the sensitivity of the response of hybrid device for the target biomarker. The target biomarker was carcinoembryonic antigen (CEA). The response of the hybrid device evidenced a linear trend from 0.1 ng/mL to 10 μg/mL, with an anionic slope of 0.1431 per decade concentration. The response of the plastic antibody for CEA revealed great selectivity against other tumour markers (CA 15–3 or CA 125). The colour response of the electrochromic cell was also CEA concentration dependent and more sensitive when the hybrid device was set-up with a photoanode with AuNPs. A more intense blue colour was obtained when higher concentrations of CEA were present.

Overall, this improved version of the self-powered and self-signalled set-up has zero-requirements and is particularly suitable for point-of-care analysis (POC). It is capable of screening CEA in real samples and differentiating clinical levels of interest. This concept opens new horizons into the current cancer screening approaches.

1. Introduction

Cancer diseases are the second cause of death worldwide (Jayanthi et al., 2017; Nair et al., 2018), with early screening being at the forefront of fighting these diseases. Current screening and diagnosis approaches include non-invasive methods as X-ray, computed tomography, resonance, and ultrasound, or more invasive procedures as biopsy (Fass, 2008; Weissleder and Pittet, 2008). From these, it is clear that the imaging approaches are expensive and time-consuming, and are not readily available after a clinician appointment (Jayanthi et al., 2017). In turn, invasive approaches are being hold back by the early biomarker detection in liquid biopsies that have clinical interest and may provide valuable information. To this end, new devices that may operate in point-of-care (POC) with low-cost, quick responses and minimal requirements are being looked for (Rasooly and Jacobson, 2006; Wu and Qu, 2015).

Aiming POC applications, electrochemical biosensors are leading the current commercial approaches. Taking the glucose meter as example, these devices allow real-time and *in-situ* measurement, along with simple, quick and low cost procedures (Grieshaber et al., 2008). In addition, these devices have small size and allow portability (Jayanthi et al., 2017; Selvolini and Marrazza, 2017). Despite these beneficial features, electrochemical biosensors still require an electrical power source to carry out measurements, which may turn out a severe limitation in places where electrical resources are limited. This has been limiting several miniaturization evolvements in electrochemical

* Corresponding author. Goreti Sales, BioMark, Sensor Research/ISEP, School of Engineering, Polytechnic Institute of Porto, R. Dr. António Bernardino de Almeida, 431, 4200-072, Porto, Portugal.
E-mail addresses: goreti.sales@gmail.com, mgf@isep.ipp.pt (M.G.F. Sales).

https://doi.org/10.1016/j.bios.2019.04.055
Received 1 March 2019; Received in revised form 24 April 2019; Accepted 29 April 2019
Available online 02 May 2019
0956-5663/

biosensing.

In terms of autonomy, electrochemical biosensors has been recently merged with a renewable electrical power source (Hong et al., 2015; Oregan and Gratzel, 1991; Truta et al., 2018; Moreira et al., 2018). In this, a Dye-sensitized Solar Cell (DSSC) is used to capture light and convert it into an electrical energy, in a concentration dependent manner. A typical DSSC contains a photoanode that is sensitive to light and a cathode that collects the electrons arriving externally from the photoanode, and sends these back to the light sensitive element through a redox electrolyte (Hagberg et al., 2008; Rho et al., 2018; Ye et al., 2014). To confer concentration dependence features to such hybrid device, the cathode of the conventional DSSC was modified with a biorecognition element sensitive to a cancer biomarker, making use of natural antibodies (Hong et al., 2015; Oregan and Gratzel, 1991; Truta et al., 2018) or as molecularly-imprinted polymers (MIPs), widely recognized as plastic antibodies (Moreira et al., 2018). Although traditionally employed in membrane separation and enrichment applications (Yoshikawa et al., 2016), MIPs have found wide use in sensing approaches, including for protein detection (Dabrowski et al., 2018). This hybrid DSSC/sensing device is therefore considered self-powered, as no electrical source is required and light is worldwide available through daylight.

This self-powered device was further evolved for an additional self-signalling feature, by using the electrical energy generated by the DSSC/sensing device and converting it into a coloured event. To this end, an electrochromic cell was interfaced in this hybrid system. The electrochromic cell generates colour in an electrically dependent manner, by means of an electrochemically induced redox reaction (Lv et al., 2017; Somani and Radhakrishnan, 2003). The electrochromic material is responsible for this feature and must change its optical properties (transmittance, absorption or reflectance) in a continuous but reversible manner upon the application of an external voltage (Beaujuge and Reynolds, 2010; Fan et al., 2016; Moser et al., 2016). An organic electrochromic material as poly(3,4-ethylenedioxythiophene) (PEDOT) is perfectly suitable for this purpose, because it is well tuned with the low energy generated by such hydride set-up (Takahashi et al., 2008; Beaujuge and Reynolds, 2010; Lv et al., 2017). However, several features may be evolved in this DSSC/sensing device.

One of these features is the sensitivity by which the device acts in a concentration dependent manner. The presence of the biorecognition element on the counter electrode decreases significantly the energy output of the DSSC, thereby decreasing the sensitivity of the overall response. This may be improved by tailoring the biorecognition element with a material that offers better electrocatalytic features to the counter electrode of the photovoltaic cell. One possibility herein includes using poly(3,4-ethylenedioxythiophene) (PEDOT), which shows good conductivity, excellent stability, and low cost (Hong et al., 2015; Yoo et al., 2014), and may be employed in the assembly of the MIP material.

In another perspective, changes in the photoanode of the DSSC may also contribute to produce a more efficient hybrid device. According to literature, a DSSC with plasmonic nanostructures on the photoanode allows the dye molecules to increase the photon absorption from sunlight (Brown et al., 2011; Guldin et al., 2010; Rho et al., 2018). Consequently, this approach shall enhance an electron flow from the dye towards the surface of the semiconductor (TiO_2), thereby increasing the photocurrent generation inside of DSSC and its energy power conversion efficiency.

Thus, the current work describes the preparation of a more efficient DSSC/hybrid device (Fig. 1), monitoring the impact of an increased power generation on the rebinding abilities of its self-powered and the self-signalled versions, by calibrating the system and retrieving both electrical and coloured data. To allow a suitable comparison to previous works, the self-powered and self-signalled device was designed to determine carcinoembryonic antigen (CEA), an important cancer biomarker in colorectal cancer (Gugov, 2005; Menaker et al., 2009). The biorecognition element is a plastic antibody, also known as a MIP material and assembled in a copolymer that also contained PEDOT. The photoanode is produced by doping the TiO_2 with gold nanoparticles (AuNPs) in order to explore their plasmonic effect. Critical variables in this context are optimized and the final system is evaluated in both buffered solutions and urine human samples, with regard to the electrical and optical output signal.

2. Materials and methods

2.1. Apparatus and materials

The general electrochemical assays were conducted in a potentiostat/galvanostat, Autolab PGSTAT302N, from Methrom, with a FRA module and interfaced in a computer by means of NOVA 1.9. Electrochemical impedance analysis (EIS) was performed in a frequency range 0.1–100000 Hz. The DSSC assays in particular also used the Autolab potentiostat, coupled to a LED driver operating with 450 mA output of a warm white LED. The photoanode was sintered in a Nabertherm GmbH P330 oven.

Solid materials were characterized by a DXR Raman spectroscope from Thermo-scientific; spectra were collected with a 785 nm excitation laser, from 47 to 3000 cm^{-1}, for 1 mW power, with a confocal aperture was set to 50 μm slit. The morphology of the films was followed by scanning electron microscopy (SEM). The digital image of the electrochromic materials was acquired by a smartphone Cink peax 2. The colour coordinates of the images belonged to the HSL colour system (Hue, Saturation and Luminousness, of the HSL space) and were collected by using the ImageJ.

The conductive glass substrates used throughout had a conductive film of fluoride-doped tin oxide (FTO, sheet resistance 13.0 Ω/sq), and were acquired to Sigma-Aldrich. The electrolyte used in Electrochromic device was a commercial Nafion solution, 20 wt% (contains alcohols) from QUINTECH.

2.2. Reagents and solutions

Ultrapure Milli-Q water was used throughout. This work required several reagents, namely potassium hexacyanoferrate III ($K_3[Fe(CN)_6]$, Riedel-de-Haën); potassium hexacyanoferrate II ($K_4[Fe(CN)_6]$, Riedel-de-Haën); phosphate buffered saline (PBS) tablets (Amresco); sodium hydrogen phosphate dihydrate ($Na_2HPO_4{\cdot}2H_2O$, Riedel-de-Haen); sodium dihydrogen phosphate dihidrate, ($NaH_2PO_4{\cdot}2H_2O$, Scharlau); 3,4-Ethylenedioxythiophene (EDOT, Alfa Aesar); potassium chloride (KCl, Merck), CEA (EastCoast Bio); proteinase k (Sigma); titanium(IV) oxide (TiO_2) nanopowder anatase phase (Sigma-Aldrich); hydrogen tetrachloroaurate (III) trihydrate ($HAuCl_4.3H_2O$, Sigma-Aldrich); ditetrabutylammonium *cis*-bis(isothiocyanato)bis(2,2′-bipyridyl-4,4′-dicarboxylato) ruthenium (II) (N719 dye, Sigma-Aldrich); lithium iodide (LiI, Sigma-Aldrich); ethanol absolute (EtOH, Sigma-Aldrich); iodine (I_2, Riedel-de-Häen); sodium borohydrate ($NaBH_4$, Riedel-de-Häen); toluene (TCI); 3-Mercaptopropylmethyldimethoxysilane (Si-SH, TCI); acetonitrile (ACN, Carlo Erba); acetone (Sigma Aldrich); pyrrol (Py, Sigma Aldrich); and glacial acetic acid (AA, Analar Normapur).

The iron redox probe solution contained 5.00×10^{-3} moL/L $K_3[Fe(CN)_6]$ and 5.00×10^{-3} moL/L $K_4[Fe(CN)_6]$, and was prepared in phosphate buffer (PB). This PB contained 0.03 moL/L of Na_2HPO_4 and 0.02 moL/L of NaH_2PO_4 (pH of 7.0). A stock standard solution of 100 μg/mL CEA was prepared in PB buffer and the less concentrated CEA standard solutions were prepared by dilution of the stock standard solution in the same buffer. The samples used herein were urine form healthy individual, with 1000 × dilution in PB buffer and spiked with CEA for concentrations ranging from 0.1 ng/mL to 100 μg/mL.

2.3. Assembly of the counter electrode

The FTO glass was successively washed with acetone, ethanol and

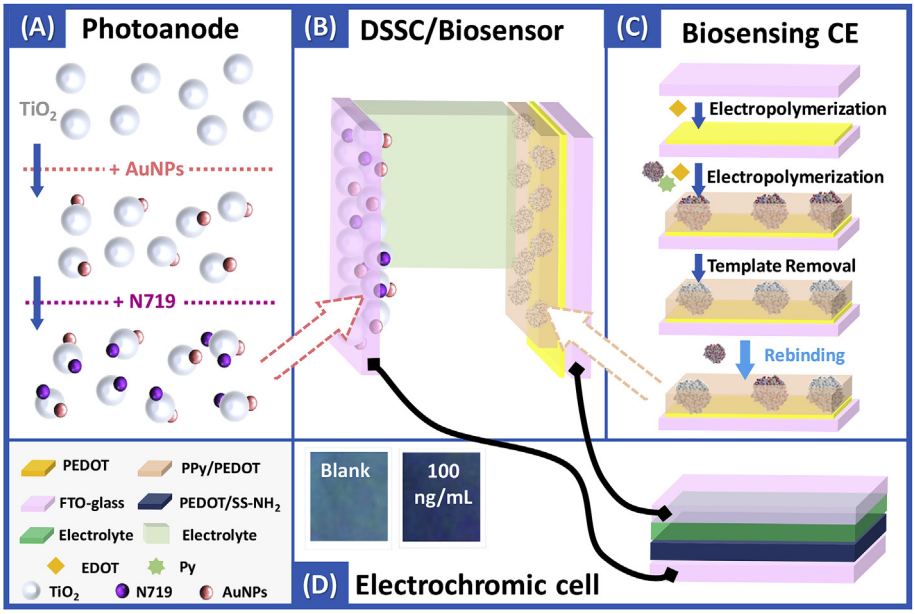

Fig. 1. Schematic representation of the several stages of the hybrid/DSSC sensor set-up with optical detection, namely the photoanode with plasmonic enhancement (A) and the biosensing counter electrode (C) combined in the DSSC cell (B), and their interface of the electrochromic cell (D).

water. Then, it was immersed in a thiol solution of Si-SH, 0.01 moL/L, prepared in toluene) to improve the adhesion of the PEDOT film to the metal oxide layer (Ouyang et al., 2017). This was made for 30 min, at 50 °C, washing after the FTO glass with ACN (Carli et al., 2014).

The next stage was the formation of a poly(EDOT) film on top (Fig. 1C), made by applying 1.10 V, for 15s, in a 3-electrodes cell dipped in a solution of 0.01 moL/L EDOT, prepared in 0.1 moL/L KCl. The final electrode (FTO/PEDOT) was also washed with ACN, to remove unreacted reagents and small oligomers.

2.4. Assembly of the imprinted film on the counter electrode

The imprinted polymer film (Fig. 1C) was assembled on top of the FTO/PEDOT glass by co-polymerizing a solution containing EDOT (0.010 moL/L) and Py (0.0020 moL/L), and also 2 µg/mL CEA, prepared in PBS (pH 7.4), by cyclic voltammetry (CV), from −0.30 V to 0.95 V, with a scan-rate of 50 mV/s, and for 10 cycles. This was done in a 3-electrodes cell, yielding an electrode that was assigned as FTO/PEDOT/MIP-CEA. After this, the CEA was extracted from the polymer using a solution of Proteinase k (500 µg/mL) overnight (FTO/PEDOT/MIP). The non-imprinted film was prepared the same way, but without CEA in the polymerizing solution (FTO/PEDOT/NIP).

2.5. Rebinding assays on the imprinted film

The rebinding of CEA (Fig. 1C) was tested in MIP or NIP films on the FTO/PEDOT electrodes. It was done by incubating buffer, standard solutions or samples in the MIP/NIP area for 20 min. First, the buffer solution was incubated consecutively until a stable signal was reached. Calibrations started by incubating the CEA standard solution of lower concentration in the surface of the material, followed by a washing step with buffer. CEA concentrations ranged from 0.1 ng/mL to 100 µg/mL, and were prepared in PB buffer, pH 7.0, or in diluted urine.

After each rebinding stage, the electrode was combined in a 3-electrodes cell to monitor the EIS data changes of a standard iron redox probe, or in a DSSC set-up to monitor the resulting photovoltaic performance. The data reported herein corresponded to a minimum of 3 independent evaluations.

2.6. Assembly of the photoanode electrode

The first step for preparing the photoanode electrode consisted in applying a homogeneous suspension of 6.0 g of TiO_2 anatase nanopowder in 10 mL of EtOH:AA:H_2O (8:1:1), on 0.7 cm^2, placed in a clean FTO glass, via doctor blade method. The electrode was then annealed at 450 °C for 30 min. After cooled down to 80 °C, the electrode was immersed in a dye solution of 5.0×10^{-4} M mol/L N719 prepared in ethanol) for 18 h, at room temperature, in the dark (Chander et al., 2014; Dembele et al., 2013; Hong et al., 2015; Mehmood et al., 2014; Truta et al., 2018). Non-adsorbed dye was removed by successive washes with EtOH. The electrode was finally dried at room temperature.

Another photoanode was prepared in parallel to evaluate the plasmonic effect of AuNPs in the DSSCs (Fig. 1A). The procedure followed for this purpose was the same, but a weight ratio of 23.9% of a colloidal AuNPs was added into the TiO_2 suspension. The AuNPs solution was prepared by the Martin method, for which 30 mL of a 2.0 mM $NaBH_4$ solution were added to 10 mL of an aqueous solutions containing 1 mM $HAuCl_4.3H_2O$ solution, under stirring and in an ice bath (Truta et al., 2019). The TiO_2 with the AuNPs were immersed in the dye solution, isolated from the exceeding reagents by annealing at 450 °C for 30 min, and cooled down.

2.7. Assembly of the DSSC

The DSSC was set-up by placing photoanode (with or without AuNPs) and CE (with or without MIP/NIP films) face-to-face, in a sandwich configuration, with a spacer in-between made from scotch magic tape (19 mm thickness). The electrical circuit was closed by placing an iodide-based electrolyte in the middle (Fig. 1B). The electrolyte solution contained 0.05 M of I_2, 0.1 M of LiI, 0.6 M of HMII and 0.5 M of TBP, dispersed in ACN.

2.8. Assembly of the electrochromic cell

The electrochromic material was a PEDOT-based film, produced in-situ by electropolymerization of EDOT of an FTO-glass support in a 3-electrodes set-up. To improve the colour change features of the final electrochromic material, 4-[2,5-Di(thiophen-2-yl)-1H-pyrrol-1-yl]aniline (SNS–NH_2) was added to the EDOT solution. SNS-NH_2 synthesis

consisted of an adaptation of the procedure made by (Ayranci et al. (2015)).

The electrochromic cell was set-up by placing face-to-face the FTO-glass with the electrochromic material and a second FTO-glass, with a polymeric electrolyte (Nafion®) in-between (Fig. 1D). It was further interfaced in the external circuit of the DSSC/sensor set-up (Fig. 1D), after ensuring that the electrochromic material was as at 0.0 V. Under working operation, the light hit the DSSC/sensor and the current generated flowed through this electrochromic cell and promoted a colour change.

2.9. Electrochemical assays

The 3-electrodes cell set-up used the previously described CEs (modified or not) as working electrode (WE), a platinum wire as auxiliary electrode (AE) and an Ag/AgCl electrode (3.4 moL/L) as reference electrode (RE). The electrochemical measurements monitored the EIS response for the redox probe $[Fe(CN)_6]^{3-/4-}$, under a standard potential of 0.22 V (± 0.01 V), with 50 scans of frequencies, and a sinusoidal potential peak-to-peak with amplitude 0.01 V in the 0.01 Hz–10000 Hz frequency range. This was done to follow-up the subsequent modifications made in the FTO glass and evaluate the impact of CEA binding on the imprinted films.

In the DSSC set-up, the *J–V* features of the cells were recorded in the potentiostat/galvanostat and used to calculate relevant photovoltaic data (overall power efficiency conversion, η; open-circuit potential, V_{OC}; short-circuit voltage, J_{SC}; and fill factor, *FF*).

The chromatic features of the electrochromic material were evaluated in a 3-electrode set-up, using 0.1 moL/L of KCl as supporting electrolyte and applying specific external potentials ranging from 0.00 V to 0.80 V.

3. Results and discussions

3.1. Assembly of sensing element on the counter electrode

3.1.1. Design of the imprinted film

The sensing film was prepared as shown in Fig. 1C. First, the FTO glass was covered by a PEDOT layer (FTO/EDOT), produced by electropolymerization at a fixed potential (1.10 V). This PEDOT layer is a suitable material to act as a CE in a conventional DSSC (Chen et al., 2007; Li et al., 2017; Song et al., 2014), and thereby shall help the interface between the photovoltaic cell and the sensing film. The imprinted film was assembled next, in a mixed solution containing EDOT, Py and CEA. The presence of EDOT in this stage is a novel approach and aim to improve the electrocatalytic features of the final electrode. As the copolymer was being formed (PEDOT and polypyrrole, PPy), the protein was entrapped within the polymeric network, yielding the formation of polymeric cavities of complementary size and shape to the template. These cavities were made accessible for rebinding of other CEA proteins, after removal of the protein template. This was successfully achieved by incubating the film in proteinase k overnight.

In order the monitor the non-specific binding ability of the polymeric network, a non-imprinted polymer (NIP) was prepared the same way, but without CEA. Such polymeric layer shall play a non-specific interaction with CEA, as there are no rebinding sites. Thus, it allows evaluating the degree of non-specific interaction established between the polymeric network and the protein itself, thereby monitoring its contribution to the overall electrochemical response.

3.1.2. SEM and Raman analysis

The modification of the CE in its several stages was followed by SEM (Figure S1), addressing the morphological changes occurring at the surface. The presence of the PEDOT layer in the FTO/PEDOT electrode was evident, when compared with the electrode with only FTO. The overall structure seemed less rough, with denser areas of PEDOT located in the deepest sites of the FTO structure. This was also confirmed by Raman spectra, made to both materials (Figure S2). The spectra of FTO/PEDOT material evidenced an obvious chemical modification, signalled by three additional peaks when compared to the FTO surface: **(1)** 1367.96, **(2)** 1437.86 and **(3)** 1506.75 cm^{-1}. These peaks are typical from PEDOT and signal their presence (Garreau et al., 1999); **(1)** was assigned to the C_β-C_β stretching, **(2)** was assigned to $C_\alpha = C_\beta$ (-O) symmetric stretching vibration; and **(3)** was assigned to the C=C asymmetric stretching of the polymeric network. Moreover, the peaks signalling the FTO surface at 559.95 cm^{-1} (Sn–O stretching vibration) and 1094.51 cm^{-1} (Si–O–Si stretching vibration and C–F stretching vibration) seemed less intense in the FTO/PEDOT material (Kumar et al., 2011; Truta et al., 2018).

The presence of additional polymer in both MIP- or NIP-based materials was also clear from the SEM images (Figure S1). Their overall surface seemed flatter, accounting the formation of these additional polymeric layers, made of PEDOT/PPy. This was especially evident in the NIP layer, which suggested that the amount of polymer formed in the NIP structure was higher than in the MIP. This was observed before, as the presence of the protein seemed to hinder the progress of the polymerization, including when electropolymerization is employed (Moreira et al., 2014). In the particular case of the MIP-based structures, a globular shape was also observed, which could signal the presence of the protein (several molecules) entrapped within the polymeric network. The are no differences evidenced between MIP after or before CEA removal, but this was likely to happen, as the magnification of the images is too little to identify the exit of the protein. In some studies, CEA has been visualized by electron microscopy and it seems like a rod shaped macromolecule with dimensions of 9 nm × 40 nm (Slayter and Coligan, 1975; Boehm et al., 1996; Schumann et al., 2004).

3.1.3. Electrochemical follow-up

The modification of the CEs for the hybrid device was followed by monitoring the charge transfer resistance (R_{ct}) of an iron redox probe in a 3-electrodes cell. The best electrical fit along the different stages of electrode modification was obtained for an equivalent Randles circuit *R*(*RQ*), in which all elements showed < 5% errors. This circuit combined the resistance of the solution, Rs, between WE (chemosensor) and RE and the Rct in parallel with a constant phase element (*Q*, related with double layer). This constant phase element behaved as a pseudo-capacitance, because the value of *Q* exponent was higher than 0.50 (Brett and Brett, 1993; Piratoba Morales et al., 2010).

In general, the FTO/PEDOT glass was a highly conductive surface, but the co-polymerization of EDOT and Py on top of it led to a less conductive material, with a much higher Rct value. This was particularly evident for the NIP material (FTO/PEDOT/NIP), as shown in Fig. 2A. In turn, the Rct value of the MIP material obtained after finishing the polymerization (FTO/PEDOT/MIP-CEA) also increased when compared to the FTO/PEDOT surface, but it was lower than that of the NIP in absolute values. As the copolymer of PEDOT/PPy had poor conductivity features and the protein CEA is a non-conductive material, it became clear that the lower Rct from the MIP film was justified by the lower amount of polymer formed, which was also consistent with the SEM images obtained (Figure S1). After template removal, an increase in Rct was observed for the MIP, which was not expected (Fig. 2B). There is no explanation for this observation, but it was a consistent behaviour, also reproducible in several assays. Remotely, this could be an outcome of the charge of the surface in the different stages; the presence of CEA on the polymeric network may have generated some positively charged locations that would attract the negatively charged iron redox probe. Upon removal of CEA, these charges would no longer exist and the redox probe would have no opposite charge interaction with the polymeric network. This increase was also partially linked to the treatment with proteinase K, as the NIP surface had the same tendency, but is a smaller extent (Fig. 2C).

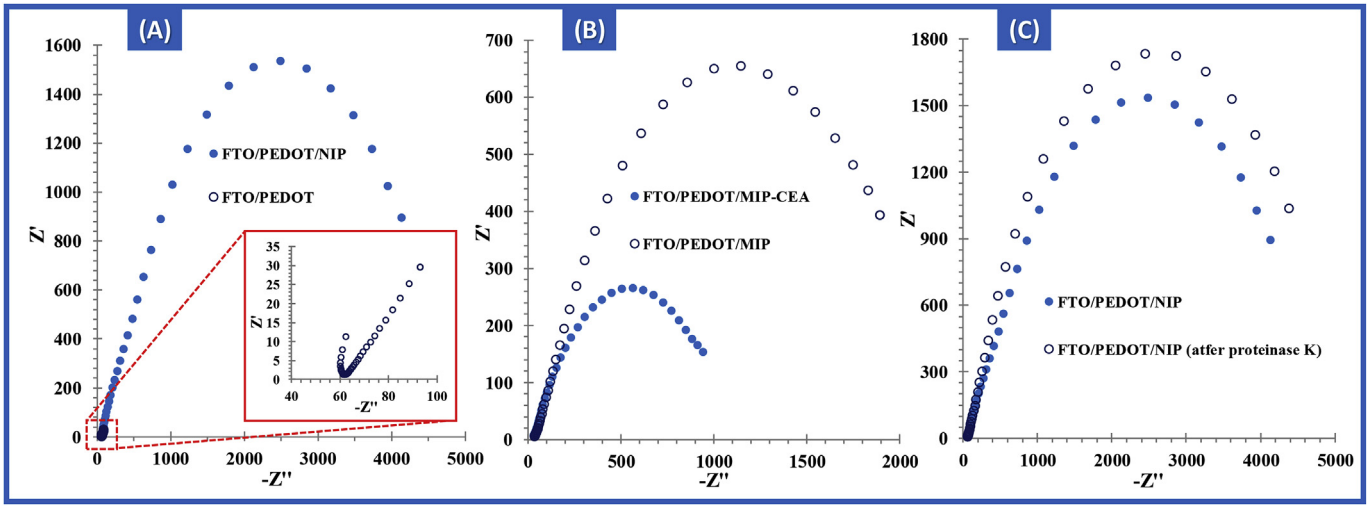

Fig. 2. Electrochemical EIS data of different steps involved in the construction of the different electrodes. (A) FTO/PEDOT glass with or without NIP. (B) MIP electrodes with or without CEA. (C) NIP electrodes with or without proteinase K treatment. Data corresponding to 5.0×10^{-3} M $K[Fe(CN)_6]^{4/3-}$ readings in PB buffer, pH 7.0.

3.2. Rebinding features of the imprinted film

The rebinding features of the imprinted film were assessed by incubating first a blank solution and CEA standard solutions of increasing concentrations on the FTO/PEDOT/MIP surface. Each incubation was made for the same time. After this, the surface was washed with PBS buffer, and incubated in the iron redox probe to check the electrochemical features on the 3-electrodes cell. As different electrodes could be used along a single calibration, the Rct signals were considered after this point as relative values (Rct') to the blank, calculated as Rct' = Rct (CEA sample)/Rct (blank). This approach was taken in assays made in a background medium of buffer or diluted urine.

The results obtained in buffer are shown in Fig. 3A, evidencing that the increasing of CEA concentration yielded an increase in the Rct value of the iron redox probe and that this increase was CEA concentration dependent (against log[CEA]). It is likely that the overall negatively charged species of CEA standing at the imprinted surface, as expected for a pH of 7.0 (Casey and Kofinas, 2008), in an increasing amount, could be increasingly avoiding the presence of the negatively charged redox probe, $[Fe(CN)_6]^{3-/4-}$.

In terms of analytical performance, it was clear that the MIP film was able to quantify very low CEA concentrations in buffered medium. The FTO/PEDOT/MIP electrode responded with a linear trend from 100 pg/mL to 10 μg/mL, showing a typical linear regression of Rct' = 0.083 × Log[CEA, ng/mL] +1.22 and a squared correlation coefficient of 0.9941; the limit of detection (LOD) was ~10 pg/mL. In contrast, the response of the corresponding NIP in the same concentration range presented a small tendency to increase, but in an uncontrolled behaviour. As shown in Figure S3 the average data obtained corresponded to a slope of 0.017 per decade concentration and a squared correlation coefficient of 0.88. Moreover, the imprinted material showed very reproducible calibration curves evaluated from independent MIP units, with the corresponding data leading to standard deviations < 7%. Consistently, the NIP showed lower reproducibility, in comparison with the MIP (also as shown in Figure S3).

Calibrations were also made in a background of diluted urine human sample, aiming to evaluate the impact of a real (complex) sample upon the electrochemical response. The typical Nyquist plots obtained under this condition are shown in Fig. 3B, and confirm a similar behaviour to that obtained in buffered solutions. The concentration of linear response was the same (0.10 ng/mL-10 μg/mL) and the slope was slightly higher, 0.1048 per decade concentration, than that of the buffer medium, which has been a typical behaviour in these kind of sensing systems (Moreira et al., 2015, 2018). Most likely, this reflects the higher ionic content of urine samples. In parallel, the control material (NIP) was also calibrated in urine dilute samples for comparison purposes. The average response so obtained is plotted in Fig. 3 (down) and evidenced little sensitivity when compared to the NIP, thereby confirming the good analytical features of the device.

Overall, the sensitivity of the MIP response was much greater than that of the NIP, for which the response was typically random. This suggested that the rebinding of CEA was controlled by the rebinding sites and that the non-specific adsorption of protein by the polymer had little impact upon the electrochemical response. Moreover, the concentration response range was within the physiological levels of interest for CEA (2.5 ng/mL and 10 ng/mL) (Duffy, 2001; Margalit et al., 2018; Nicholson et al., 2016).

3.3. Integrating the imprinted film on the DSSC

3.3.1. The set-up

The impact of the imprinted film upon the DSSC was monitored by evaluating the photovoltaic features of DSSCs assembled with CEs of FTO/PEDOT, FTO/PEDOT/MIP-CEA and FTO/PEDOT/MIP (Fig. 4A).

The main features of the DSSC operating with a conventional FTO/PEDOT CE included an efficiency (η) of 2.80%, a density short circuit (J_{SC}) of 5.93 mA/cm^2 and a fill factor (FF) value of 66.90%. The preparation of the imprinted material on top of this electrode, also including the CEA protein within the polymeric network, was responsible for a ~63% decrease in the overall efficiency of the DSSC cell down to 1.02% η, which was also consistent with the data in Fig. 2A. The other photovoltaic parameters, J_{SC}, FF and P_{max} also decreased to 4.79, 32.40 and 0.65, respectively. After template removal (FOT/PEDOT/MIP), the efficiency decreased again, down to 0.55%, a behaviour that was also consistent with the results shown in Fig. 2B, in which the exit of the protein almost doubled the Rct value obtained. Yet, the overall output of the cell was however better than that obtained with a CE having only PPy and MIP material. There was a slightly lower LOD presented herein (0.11 ng/mL), comparing with LOD of PPy MIP (0.14 ng/mL); moreover, a wider linear range was observed in this work, 0.1 ng/mL until 100 μg/mL, against a narrower linear range of PPy MIP (100 ng/mL to 100 μg/mL).

3.3.2. Rebinding features on the hybrid set-up

The MIP electrode operating as the CE of a DSSC gets in contact with an iodide redox probe prepared in ACN, which is quite different from

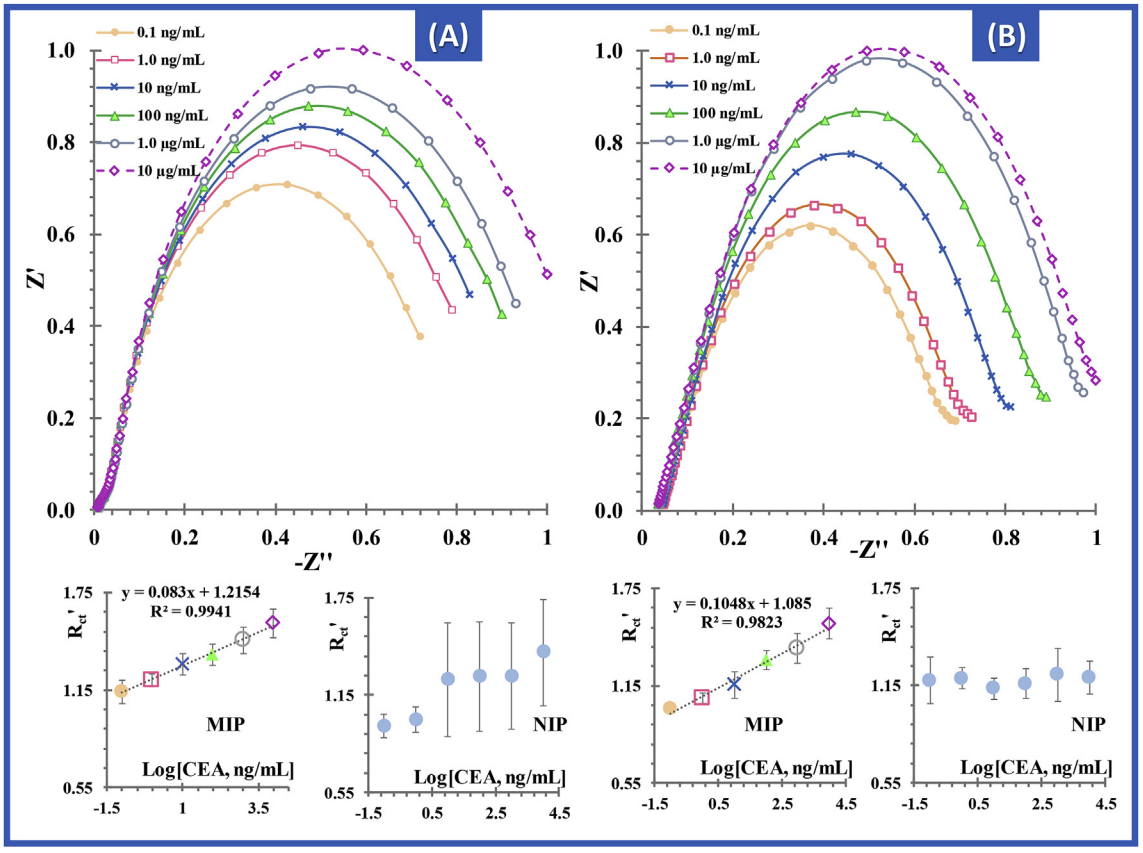

Fig. 3. Nyquist plots (top) of the FTO/PEDOT/MIP electrode in a 3-eletrodes cell, with a 5.0×10^{-3} M $[Fe(CN)_6]^{4/3-}$ redox probe, prepared in PB buffer, pH 7.0, after incubation of increasing concentrations of CEA solutions prepared in buffer (A) or in diluted sample solution (B), and the corresponding calibration curves (down) as relative Rct versus log[CEA], also including the average values obtained for the FTO/PEDOT/NIP electrode.

the typical iron redox probe prepared buffer, used in the 3-electrodes cell evaluation. The impact of this new electrolyte in the rebinding of CEA in terms of photovoltaic operation should therefore be monitored. As in previous studies, these rebinding studies were made in both buffered solutions and diluted urine samples, for CEA concentrations ranging from 0.1 ng/mL to 100 µg/mL.

The power curves obtained for each incubated concentration level are shown in Fig. 5, and revealed a decreased performance of the photovoltaic cell for increasing amounts of CEA adsorbed to the MIP film. This was consistent with the data shown in Fig. 3, in which the Rct increased for increasing concentrations of CEA. Moreover, the DSSC set-up was also sensitive to CEA within the same concentration range as the MIP film, evaluated in the 3-electrodes cell. In buffered solutions (Fig. 5A), the linear behaviour observed for relative η ($\eta' = \eta_{sample}/\eta_{blank}$) against log[CEA] showed a typical anionic slope of 0.0757 per decade concentration and a square correlation coefficient > 0.995.

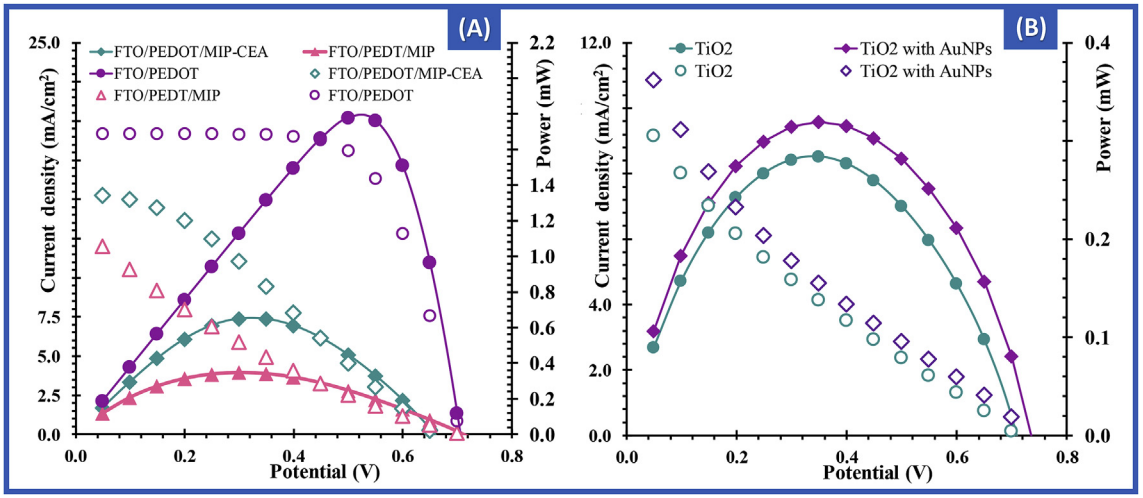

Fig. 4. – Photocurrent density-photovoltage (*J-V*) and power conversion efficiency characteristic curves of DSSCs assembled (A) with different CEs (FTO/PEDOT, FTO/PEDOT/MIP-CEA or FTO/PEDOT/MIP) and a photoanode of TiO_2 sensitized with N719; or assembled (B) with different photoanodes, with or without AuNPs, and a CE of FTO/PEDOT/MIP. Studies made with an electrolyte of I^-/I_3^-.

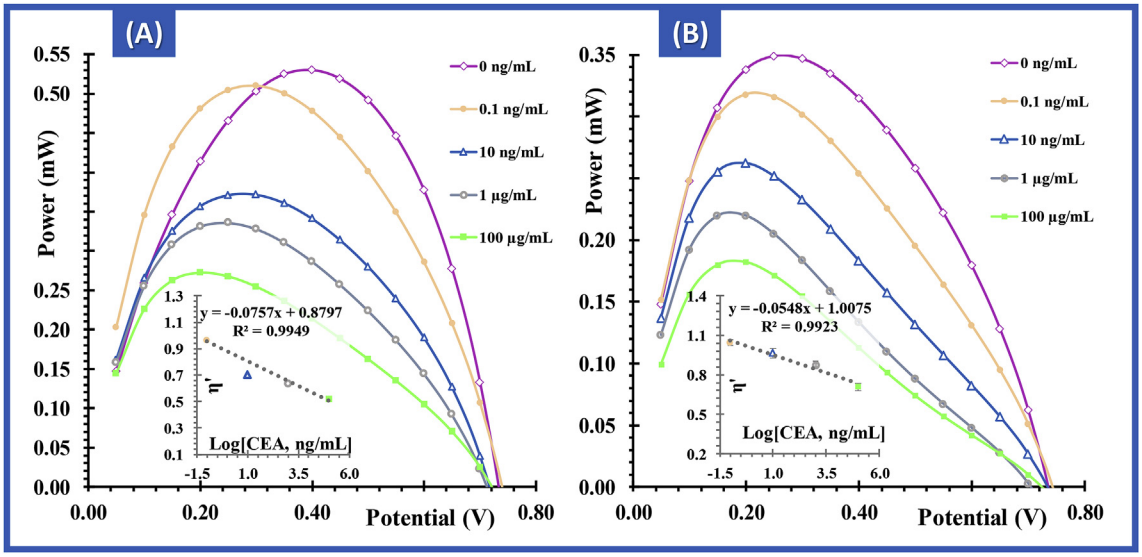

Fig. 5. Power curves and the corresponding calibration curves (inset, as relative η versus log[CEA]) of the FTO/PEDOT/MIP electrode in the DSSC set-up, after incubating increasing concentrations of CEA solutions, prepared in buffer (A) or in diluted sample solution (B). DSSC with a photoanode of TiO_2 and an electrolyte of I^-/I_3^-.

Other photovoltaic parameters of this system (as V_{OC}, J_{SC} and FF) were also plotted against the log[CEA], but a lower quality linear trend was obtained. The LOD of this system was 0.11 ng/mL. In diluted urine solutions (Fig. 5B), the photovoltaic parameters presented similar changes when compared to the assays in buffer. The typical anionic slope for η' against log[CEA] was 0.055 per decade concentration and the square correlation coefficients were > 0.992.

Overall, the analytical response of the MIP film inside the DSSC was observed from 0.1 ng/mL to 100 µg/mL, the same concentration range of linear response in the 3-electrodes cell and using a different redox probe. In general, the system responded with a reasonable sensitivity. The slope generated by CEA solutions in urine was however slightly smaller than the one observed in buffered solutions. This was an outcome of the decreased absolute power promoted by the blank urine samples. Although not questioning the analytical usefulness of this set-up, this decreased sensitivity revealed the great impact generated by the absolute efficiency of the cell when in the blank solution. This value was interfering with the overall sensitivity of the analytical system, being therefore important to identify a strategy that would increase such efficiency value.

3.4. Enhancing the DSSC/chemosensor efficiency

The addition of plasmonic nanomaterials to the photoanode has been identified as a way to improve the energy generated by DSSCs (Brown et al., 2011; Guldin et al., 2010; Rho et al., 2018; Truta et al., 2019). For this purpose, a novel photoanode was prepared by adding metal nanoparticles of gold (AuNPs) into the conventional semiconductor (TiO_2) support, while keeping the same active area of the photoactive layer in the previous electrodes (0.7 cm^2). The presence of Au in the TiO_2 photoanode was confirmed by SEM analysis (Figure S4), with a backscattered electron detector, ensuring different intensities and contrasts according to the atomic number of Ti and Au (Lloyd, 1987), and by the EDS analysis. The set-up made to evaluate this feature used the FTO/PEDOT/MIP material as CE.

The *J-V* measurements made are shown in Fig. 4B and were used to calculate the corresponding photovoltaic performance, expressed as J_{SC}, V_{OC}, FF, and η. This data is summarized in Table S1. An increase in J_{SC} from 3.10 to 3.80 mA/cm^2 was observed, when DSSC was assembled with photoanode of TiO_2 and AuNPs, which corresponded to a 22.3% increase. Moreover, the photoanode with AuNPs displayed a better efficiency (η = 0.504%) than the photoanode with only semiconductor. Overall, it was possible to observe that the performance of DSSCs improved when the Au nanoparticles were introduced in the TiO_2 paste. This derived from the plasmonic effect of such NPs, which enhance the light absorption that hits the cell according to (Brown et al., 2011; Guldin et al., 2010; Rho et al., 2018).

The impact of this power increase on the analytical features of the DSSC/sensor hybrid device was also monitored by re-evaluating the rebinding features in diluted urine samples, using this set-up. The *J-V* measurements obtained under this condition are shown in Fig. 6A. Overall, the average anionic slope obtained by using a photoanode with AuNPs was 0.1431 per decade concentration, corresponding to a higher value than that without AuNPs (Fig. 6B). The calibrations made were also linked to a wider relative η change; it varied from 0.9 to 0.2, from the lowest to the highest concentration, meaning that the range of the operational useful analytical signal was also amplified by using a photoanode with AuNPs. Similar to previous experiences, the photovoltaic parameters also decreased when the concentration of CEA increased along the calibration procedure, but their linear fit with the log [CEA] was not as evident as the η'. A control material was also evaluated against CEA concentration in DSSC/sensor hybrid device using a photoanode with AuNPs. It showed decreasing η' values along the calibration procedure, when exposed to the same conditions as the MIP. Yet, the sensitivity of the NIP was lower than that of the MIP, evidencing an anionic slope of 0.069, with a correlation coefficient of 0.9287 (Figure S5).

Overall, the DSSC/sensor hybrid system operating with a plasmonic effect from AuNPs favoured the sensitivity of response against CEA concentration. First, the power of the blank signal increased and, second, the value of η' before saturation was lower than that with photoanodes without plasmonic nanostructures. This wider range of electrical response would most certainly favour the response of the signalling element, another aspect presented next.

3.5. Selectivity of DSSC/sensor

The selectivity test evaluated the effect of chemical compounds that could be potential interfering compounds in biological fluids. This was achieved by a competing test between CEA (in 50 ng/mL) and other interfering species selected for this propose. Herein, the tumour biomarkers, CA 15.3 and CA 125 and urea, the most abundant compound

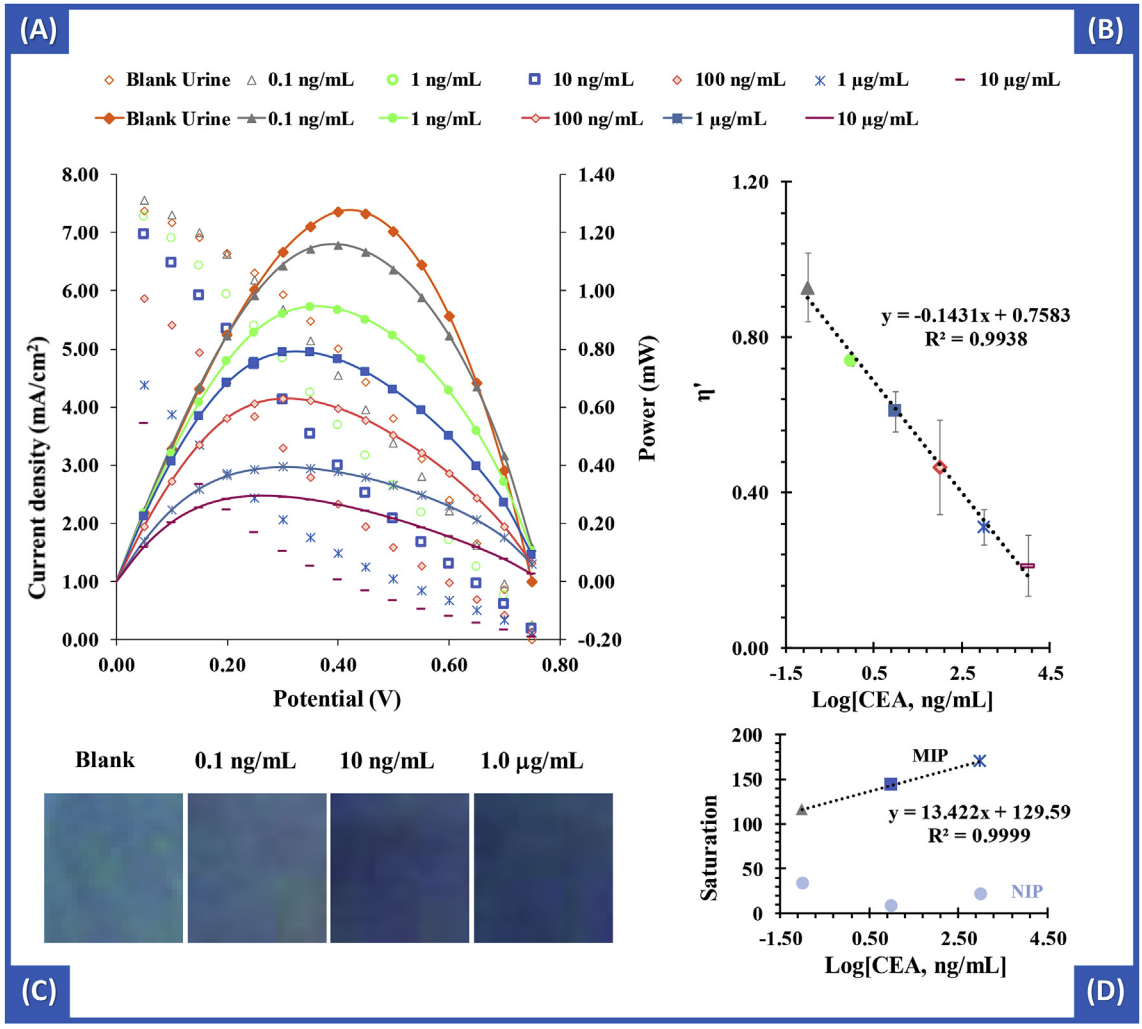

Fig. 6. Power curves (A) of the FTO/PEDOT/MIP electrode in the DSSC set-up containing a photoanode with AuNPs, after incubation in increasing concentrations of CEA solutions, prepared in diluted urine sample solution, (B) the corresponding calibration plots as η′ versus log[CEA], along with the colour generated by the electrochromic cell (C) and the corresponding saturation coordinate of the HSL colour system against log[CEA]. (For interpretation of the references to colour in this figure legend, the reader is referred to the Web version of this article.)

in urine, were selected. The concentrations used for this purpose were 1.6 U/mL, 2.5 U/mL, and 1.2 mg/mL respectively, considering a possible 10 × dilution of an original serum sample.

Selectivity studies were evaluated in two different conditions, using binary (CEA + interfering species) or single component (only interfering species) solutions. Each solution was incubated in the sensing layer (CE) for 20 min, the same period used in the calibration procedure. The results obtained with the binary solutions were compared to those of a single component CEA solution. The data obtained is shown in Figure S6, evidencing that the tested compounds did not interfere significantly with the CEA readings, changing the signal from 4.1 to 15.5% (Figure S6). Using single component solutions, each compound was incubated separately and the results indicated a low rebinding ability for CA 15.3 (15.3%), CA 125 (3.4%) or urea (23%), when compared to CEA (Figures S7 and S8). These values are corresponding to the worst scenario, because there was no other ion competing for the sensing layer with the interfering compound, which may allow a significant non-specific rebinding response.

Overall, the results obtained evidenced the very good selectivity features of the MIP sensing layer, confirming that the chemosensor had a high affinity for the target molecule.

3.6. Inclusion of the self-signalling element

3.6.1. Interface with the electrochromic cell

The self-signalling element consisted of an electrochromic cell (Fig. 1D) linked to the external circuit of the DSSC/sensor. This cell was set-up according with an organic electrochromic material of PEDOT and SNS-NH_2, and changed its colour in agreement with the energy arriving from the hybrid device. As the energy produced by the hybrid photovoltaic cell was CEA concentration dependent, it was reasonable to assume that the electrochromic material would yield colour differences under increasing CEA concentrations.

For this purpose, rebinding studies were made as previously on the FTO/PEDOT/MIP electrode, which was handled after as the CE of a DSSC cell equipped with a photoanode containing AuNPs. The concentrations selected for this purpose were 0.10 ng/mL, 10 ng/mL, 1.0 µg/mL and 100 µg/mL, the same concentration range tested before. After rebinding, each MIP electrode was combined with the photoanode and the necessary electrolyte to generate a given current that should be in agreement with the CEA concentration. This current flowed through the electrochromic cell (Fig. 1), and a total of 12 min was given to reach a stable colour.

The colours obtained for the different concentrations in urine sample solutions are shown in Fig. 6C. The blank signal corresponds to

the incubation of diluted urine sample with no CEA, and yielded the highest power produced by the hybrid device and feeding the electrochromic cell. The corresponding colour was typical light blue, which seems to correspond to the colour promoted by potentiostatic response under 0.7 V applied in 3-electrode cell configuration (Figure S9). Increasing CEA concentrations incubated in the MIP CE up to 1.0 μg/mL yielded decreasing currents, which were linked to the formation of a darker blue colour in the electrochromic cell. The highest concentration of all, 100 μg/mL, led to no colour variation, meaning that the current arriving at this point at the electrochromic cell was insignificant and unable to promote additional colour changes. Overall, the colours observed for increasing CEA concentrations were in a clear gradient change (original pictures in Figure S10), which was visually perceptible.

The direct impact of using a more efficient hybrid device upon the colour change was also assessed, by carrying out the same assays in a DSSC with a photoanode without AuNPs. The colours produced were less intense and tended to purple instead of a dark blue colour (Figure S11). The saturation was not reached in the complete concentration range, probably because in this configuration the power decrease for CEA increasing concentrations was less intense, thereby reaching less quickly a near close-to-zero power condition. Overall, this data confirmed the great relevance of using a more efficient cell in the coloured transduction of the rebinding event.

The gradient observed was also used to extract quantitative data, in a similar way to the approach reported by (Gomes and Sales, 2015). To this end, the colour coordinates of the HSL (Hue, Saturation and lightness) colour system were extracted by the ImageJ. The collected values were tested against the log CEA concentration, to find the possibility of having a linear trend between these. The best mathematical fit plotted y-axis as saturation (Figure S12), against the log CEA concentration, yielding the linear trend observed in Fig. 6D.

Overall, it was evidenced that the visual inspection of the colour changes in the electrochromic cell provided semi-quantitative data (Fig. 6C and Figure S11) and that this data could be further refined to generate quantitative evidence. In general, all data produced was clinically relevant, but the use of the DSSC with AuNPs may clearly benefit the generation of more accurate data, as the colour change was more intense.

4. Conclusions

This work confirmed the possibility of producing effective self-powered and self-signalled sensing devices for CEA, by merging different technologies. Photovoltaic cells, plastic antibodies (or MIP technology), plasmonic nanomaterials and electrochromic cells were combined to target an electrochemical detection system that retrieves a coloured response. In this new format, the photovoltaic cell was responsible to generate power to the electrochemical device and acted in a concentration dependent manner, when one of its electrodes was modified with plastic antibodies. This power crossed the electrochromic cell that converted this energy into a coloured event; as the intensity of the formed colour was power dependent, the observed colour was is turn concentration dependent, thereby enabling visual detection. The plasmonic nanomaterials were tested herein as an additional element into this system that could improve the performance of the photovoltaic cell and contributed to an increased sensitivity, interestingly revealed by an improved coloured detection.

From a practical perspective, the hybrid device was able to respond to CEA concentrations between 0.1 ng/mL-10 μg/mL, which is an important range for disease screening, diagnosis or progression, and the use of plasmonic AuNPs yielded an improved sensitivity. It generated semi-quantitative data by simple visual inspection of the colour gradient, but the colour coordinates could be used to generate quantitative information. Moreover, the current device has a single light requirement and offers the potential to generate relevant data for clinical decision, in a fully independent manner, everywhere. In principle, the concept behind this hybrid device may eventually be extended to any other target biomolecule.

5. Credit author statement

Photovoltaics, plasmonics, plastic antibodies and electrochromism combined for a novel generation of self-powered and self-signalled electrochemical biomimetic sensors, Ana P.M. Tavares, Liliana A.A.N.A. Truta, Felismina T.C. Moreira, Graça Minas, M. Goreti F. Sales.

Ana P.M. Tavares: investigation in the biomimetic sensor and the electrochromic cell, data curation, methodology, validation, and writting original draft. Liliana A.A.N.A. Truta: investigation in DSSCs, data curation. Felismina T.C. Moreira: supervision, investigation in biorecognition elements, data curation, and draft review and editing. Graça Minas: supervision of the electronic part of the work, and draft reviewing and editing. Goreti Sales: conceptualization, funding acquisition, overall supervision, project administration, and draft review and editing.

Declaration of interests

- The authors declare that they have no known competing financial interests or personal relationships that could have appeared to influence the work reported in this paper.
- The authors declare the following financial interests/personal relationships which may be considered as potential competing interests:

Acknowledgements

The authors acknowledge the financial support of European Research Council though the Starting Grant, 3P's Starting Grant/ERC (GA 311086).

Appendix A. Supplementary data

Supplementary data related to this article can be found at https://doi.org/10.1016/j.bios.2019.04.055.

References

Ayranci, R., Demirkol, D.O., Ak, M., Timur, S., 2015. Sensors 15 (1), 1389–1403.
Beaujuge, P.M., Reynolds, J.R., 2010. Chem. Rev. 110 (1), 268–320.
Boehm, M.K., Mayans, M.O., Thornton, J.D., Begent, R.H., Keep, P.A., Perkins, S.J., 1996. J. Mol. Biol. 259 (4), 718–736.
Brett, C.M.A., Brett, A.M.O., 1993. Electrochemistry: Principles, Methods, and Applications. Oxford Science Publications, Oxford University.
Brown, M.D., Suteewong, T., Kumar, R.S.S., D'Innocenzo, V., Petrozza, A., Lee, M.M., Wiesner, U., Snaith, H.J., 2011. Nano Lett. 11 (2), 438–445.
Carli, S., Casarin, L., Bergamini, G., Caramori, S., Bignozzi, C.A., 2014. J. Phys. Chem. C 118 (30), 16782–16790.
Casey, B.J., Kofinas, P., 2008. J. Biomed. Mater. Res. A 87A (2), 359–363.
Chander, N., Khan, A.F., Thouti, E., Sardana, S.K., Chandrasekhar, P.S., Dutta, V., Komarala, V.K., 2014. Sol. Energy 109, 11–23.
Chen, J.-G., Wei, H.-Y., Ho, K.-C., 2007. Sol. Energy Mater. Sol. Cells 91 (15–16), 1472–1477.
Dabrowski, M., Lach, P., Cieplak, M., Kutner, W., 2018. Biosens. Bioelectron. 102, 17–26.
Dembele, K.T., Nechache, R., Nikolova, L., Vomiero, A., Santato, C., Licoccia, S., Rosei, F., 2013. J. Power Sources 233, 93–97.
Duffy, M.J., 2001. Clin. Chem. 47 (4), 624–630.
Fan, M.S., Kao, S.Y., Chang, T.H., Vittal, R., Ho, K.C., 2016. Sol. Energy Mater. Sol. Cells 145, 35–41.
Fass, L., 2008. Mol. Oncology 2 (2), 115–152.
Garreau, S., Louarn, G., Buisson, J.P., Froyer, G., Lefrant, S., 1999. Macromolecules 32 (20), 6807–6812.
Gomes, H.I.A.S., Sales, M.G.F., 2015. Biosens. Bioelectron. 65, 54–61.
Grieshaber, D., MacKenzie, R., Voros, J., Reimhult, E., 2008. Sensors 8 (3), 1400–1458.
Gugov, T., 2005. Stanford University.
Guldin, S., Hüttner, S., Kolle, M., Welland, M.E., Müller-Buschbaum, P., Friend, R.H., Steiner, U., Tétreault, N., 2010. Nano Lett. 10 (7), 2303–2309.
Hagberg, D.P., Yum, J.H., Lee, H., De Angelis, F., Marinado, T., Karlsson, K.M., Humphry-Baker, R., Sun, L.C., Hagfeldt, A., Gratzel, M., Nazeeruddin, M.K., 2008. J. Am. Chem.

Soc. 130 (19), 6259–6266.
Hong, C.K., Ko, H.S., Han, E.M., Park, K.H., 2015. Int. J. Electrochem. Sci. 10 (7), 5521–5529.
Jayanthi, V.S.P.K.S., Das, A.B., Saxena, U., 2017. Biosens. Bioelectron. 91, 15–23.
Kumar, V., Govind, A., Nagarajan, R., 2011. Inorg. Chem. 50 (12), 5637–5645.
Li, Y.-C., Jia, S.-R., Liu, Z.-Y., Liu, X.-Q., Wang, Y., Cao, Y., Hu, X.-Q., Peng, C.-L., Li, Z., 2017. J. Mater. Chem. 5 (17), 7862–7868.
Lloyd, G.E., 1987. Mineral. Mag. 51 (359), 3–19.
Lv, X., Li, W., Ouyang, M., Zhang, Y., Wright, D.S., Zhang, C., 2017. J. Mater. Chem. C 5 (1), 12–28.
Margalit, O., Mamtani, R., Yang, Y.-X., Reiss, K.A., Golan, T., Halpern, N., Aderka, D., Giantonio, B., Shacham-Shmueli, E., Boursi, B., 2018. Eur. J. Cancer 94, 1–5.
Mehmood, U., Rahman, S., Harrabi, K., Hussein, I., Reddy, B.V., 2014. Ann. Mater. Sci. Eng. 1–12.
Menaker, A., Syritski, V., Reut, J., Opik, A., Horvath, V., Gyurcsanyi, R.E., 2009. Adv. Mater. 21 (22), 2271.
Moreira, F.T.C., Sharma, S., Dutra, R.A.F., Noronha, J.P.C., Cass, A.E.G., Sales, M.G.F., 2014. Sens. Actuators, B 196, 123–132.
Moreira, F.T.C., Sharma, S., Dutra, R.A.F., Noronha, J.P.C., Cass, A.E.G., Sales, M.G.F., 2015. Microchim. Acta 182 (5), 975–983.
Moreira, F.T.C., Truta, L.A.A.N.A., Sales, M.G.F., 2018. Sci. Rep. 8 (1), 10205.
Moser, M.L., Li, G.H., Chen, M.G., Bekyarova, E., Itkis, M.E., Haddon, R.C., 2016. Nano Lett. 16 (9), 5386–5393.
Nair, M., Sandhu, S.S., Sharma, A.K., 2018. Semin. Canc. Biol. 52 (Part 1), 39–55.
Nicholson, B.D., Shinkins, B., Mant, D., 2016. J. Am. Med. Assoc. 316 (12), 1310–1311.
Oregan, B., Gratzel, M., 1991. Nature 353 (6346), 737–740.
Ouyang, L., Wei, B., Kuo, C.-c., Pathak, S., Farrell, B., Martin, D.C., 2017. Sci. Adv. 3 (3), e1600448.
Piratoba Morales, U., Vera Lopez, E., Ortiz Otalora, C., 2010. Dyna-Colombia 77 (162), 13–19.
Rasooly, A., Jacobson, J., 2006. Biosens. Bioelectron. 21 (10), 1851–1858.
Rho, W.-Y., Song, D.H., Yang, H.-Y., Kim, H.-S., Son, B.S., Suh, J.S., Jun, B.-H., 2018. J. Solid State Chem. 258, 271–282.
Schumann, D., Huang, J., Clarke, P.E., Kirshner, J., Tsai, S.W., Schumaker, V.N., Shively, J.E., 2004. Biochem. Biophys. Res. Commun. 318 (1), 227–233.
Selvolini, G., Marrazza, G., 2017. Sensors 17 (4).
Slayter, H.S., Coligan, J.E., 1975. Biochemist 14 (11), 2323–2330.
Somani, P.R., Radhakrishnan, S., 2003. Mater. Chem. Phys. 77 (1), 117–133.
Song, D., Li, M., Wang, T., Fu, P., Li, Y., Jiang, B., Jiang, Y., Zhao, X., 2014. J. Photochem. Photobiol., A 293, 26–31.
Takahashi, Y., Hayashi, N., Oyaizu, K., Honda, K., Nishide, H., 2008. Polym. J. 40 (8), 763–767.
Truta, L.A.A.N.A., Moreira, F.T.C., Sales, M.G.F., 2018. Biosens. Bioelectron. 107, 94–102.
Truta, L.A.A.N.A., Pereira, S., Hora, C., Trindade, T., Sales, M.G.F., 2019. Electrochim. Acta 300, 102–112.
Weissleder, R., Pittet, M.J., 2008. Nature 452 (7187), 580–589.
Wu, L., Qu, X.G., 2015. Chem. Soc. Rev. 44 (10), 2963–2997.
Ye, M., Wen, X., Wang, M., Iocozzia, J., Zhang, N., Lin, C., Lin, Z., 2014. Mater. Today 18 (3).
Yoo, D., Kim, J., Kim, J.H., 2014. Nano Res 7 (5), 717–730.
Yoshikawa, M., Tharpa, K., Dima, S.O., 2016. Chem. Rev. 116 (19), 11500–11528.